

Higher-Order Energy-Decreasing Exponential Time Differencing Runge–Kutta methods for Gradient Flows

Zhaohui Fu¹, Jie Shen², and Jiang Yang^{3,4}

¹Department of Mathematics, National University of Singapore, Singapore(fuzhmath@gmail.com)

²School of Mathematical Science Eastern Institute of Technology, Ningbo, Zhejiang 315200, P. R. China (jshen@eitech.edu.cn)

³Department of Mathematics, SUSTech International Center for Mathematics & National Center for Applied Mathematics Shenzhen (NCAMS), Southern University of Science and Technology, Shenzhen, China (yangj7@sustech.edu.cn)

February 26, 2024

Abstract

We develop in this paper a general framework for constructing higher-order, unconditionally energy-stable exponential time differencing Runge–Kutta (ETDRK) methods applicable to a large class of gradient flows. Specifically, we identify a set of sufficient conditions that ETDRK schemes need to satisfy to maintain the original energy dissipation. Our analysis reveals that commonly used third-order and fourth-order ETDRK schemes fail to meet these conditions, and we construct new third-order ETDRK schemes which satisfy these conditions and thus guarantee the unconditional energy dissipation. We conduct extensive numerical experiments with these new schemes to verify their accuracy, stability, behavior under large time steps, long-term evolution, and adaptive time stepping strategy for various gradient flows.

Keywords: exponential time differencing Runge–Kutta method; energy stability; gradient flows; phase-field models

AMS subject classification (2020): 65M12; 35K20; 35K35; 35K55

1 Introduction

We consider a class of gradient flows written in the following general form

$$u_t = G(\mathcal{L}u + f(u)), \quad (x, t) \in \Omega \times [0, T], \quad (1.1)$$

where Ω is a bounded domain in R^d ($d = 1, 2, 3$), T is a finite time, G is a negative operator, \mathcal{L} is a sectorial operator. The above system is energy dissipative with corresponding energy functional

$$E(u) = \int_{\Omega} \left(\frac{1}{2} |\mathcal{L}_{1/2} u|^2 + F(u) \right) dx, \quad (1.2)$$

where $\mathcal{L}_{1/2}\mathcal{L}_{1/2}^* = \mathcal{L}_{1/2}^*\mathcal{L}_{1/2} = \mathcal{L}$ and $F' = f$. This general form covers a wide range of gradient flows, such as the Allen–Cahn equation, the Cahn–Hilliard equation, the thin film model without slope selection also known as the molecular beam epitaxy (MBE) model, the phase-field crystal models and etc.

Since these gradient flows involve strong nonlinearities and often with high-order derivatives, it is difficult to design an efficient time discretization scheme which is able to accurately approximate their dynamics and steady states. In particular, it is challenging for numerical schemes to guarantee the energy decay which is intrinsic to all of these models. Ample numerical evidences indicate that non-physical oscillations may occur when the energy stability is violated. Furthermore, the establishment of unconditional energy stability enables the creation of more efficient algorithmic designs, including the development of adaptive time stepping strategies, where the selection of time steps is solely governed by considerations of accuracy.

There have been a large amount of studies concerning energy stable schemes for gradient flows, see, e.g. [9, 12, 10, 27, 30, 32, 28, 16, 18] and the references therein. In particular, the convex splitting technique [29, 25] is useful to preserve unconditional energy stability, but it leads to a nonlinear scheme and not easy to extend it to more general cases. The invariant energy quadratization (IEQ) method (see, e.g. [34, 35]) and the scalar auxiliary variable (SAV) method [4, 26] lead to linear schemes which can preserve different structures for a wide class of gradient flows. In particular, there have been a large number of works based on SAV methods, including SAV-BDF schemes [17, 3] and SAV-RK schemes [1, 31]. However, the energy stability achieved by the IEQ or SAV methods is based on a modified energy, not the original energy. We are not aware of any linear and higher than second-order scheme for (1.1) could be unconditional energy stable with respect to the original energy.

On the other hand, exponential time differencing Runge–Kutta (ETDRK) schemes offer many advantages over multistep methods. In this paper, we consider exponential time differencing Runge–Kutta (ETDRK) methods for (1.1). The key idea of ETDRK schemes is to apply the Duhamel’s principle

$$u(x, t) = e^{G\mathcal{L}(t-t_0)}u(x, t_0) - e^{G\mathcal{L}(t-t_0)} \int_{t_0}^t e^{-G\mathcal{L}(s-t_0)} Gf(u(x, s)) ds, \quad (1.3)$$

and approximate the implicit integral which contains the unknown $f(u(x, s))$ with an explicit RK method. The concept of exponential integrators has a long-standing history, tracing its origins back to the 1960s. There has been much literature related to using such methods to solve stiff problems, semilinear parabolic problems or gradient flows [6, 8, 11, 14, 5]. However, ETDRK schemes are usually not energy stable. It has been shown in [6, 7] that some first-order ETDRK schemes can be energy stable. More recently, it is shown in [11] that a second-order ETDRK scheme, with proper stabilization, is unconditional energy stable. However, no higher than second-order ETDRK scheme has proven to be energy stable.

This paper aims to introduce a comprehensive framework for developing unconditionally energy-stable ETDRK schemes tailored for various gradient flows. Our main contributions include

- We have formulated a series of criteria for ensuring the unconditional energy stability of ETDRK schemes, irrespective of their order, see Theorem 2.1.

- Our investigations reveal that the widely employed third-order and fourth-order ETDRK methods are not energy stable, and we have constructed new third-order ETDRK schemes that satisfy the criteria in Theorem 2.1, thereby achieving unconditional energy stability.

We are optimistic that the foundational framework proposed in this paper will pave the way for the creation of more advanced energy stable ETDRK schemes.

This paper is organized as follows. In Section 2, we present some background knowledge, then state and prove our main theorem. In Section 3, we apply the main theorem to various known ETDRK schemes and determine whether they are unconditional energy stable, in particular, we show that the commonly used third-order and fourth-order ETDRK schemes do not satisfy these conditions, and we construct new third-order ETDRK schemes which satisfy these conditions and thus are unconditional energy stable. In Section 4, we presents ample numerical experiments to validate our new third-order schemes, and to study how large time steps affect the solutions, how different time steps and stabilizers influence the energy evolution, we also present an example with adaptive time stepping. Some concluding remarks are given in the final section.

2 Energy decreasing ETDRK methods for gradient flows

In this section we first introduce some basic knowledge for gradient flows and some phase field models, convex splitting and the ETDRK methods. Then we prove our main theorem, i.e. arbitrary ETDRK schemes are unconditionally energy stable as long as the conditions are satisfied.

2.1 Phase-field models

We consider the general form of gradient flows in a Hilbert space \mathcal{H} with inner product (\cdot, \cdot) and norm $\|\cdot\|$:

$$u_t = G(\mathcal{L}u + f(u)), \quad (x, t) \in \Omega \times [0, T], \quad (2.1)$$

where G is a negative operator, \mathcal{L} is a symmetric sectorial operator, and $f(u) = F'(u)$, where $F(u)$ is a nonlinear functional. Taking the inner product of (2.1) with $\mathcal{L}u + f(u)$, we find the energy dissipation law

$$\frac{d}{dt}E(u) = (G(\mathcal{L}u + f(u)), \mathcal{L}u + f(u)) \leq 0, \quad (2.2)$$

where the free energy $E(u)$ is given by

$$E(u) = \int_{\Omega} \left(\frac{1}{2}(\mathcal{L}u, u) + F(u) \right) dx. \quad (2.3)$$

Some typical examples are:

- the Allen–Cahn equation, $G = -1$, $\mathcal{L} = -\epsilon^2\Delta$, $f(u) = u^3 - u$ and $F(u) = \frac{1}{4}(u^2 - 1)^2$;
- the Cahn–Hilliard equation, $G = \Delta$, $\mathcal{L} = -\epsilon^2\Delta$, $f(u) = u^3 - u$ and $F(u) = \frac{1}{4}(u^2 - 1)^2$;
- the MBE model without slope selection, $G = -1$, $\mathcal{L} = -\epsilon^2\Delta^2$ but $f(u)$ should be replaced by $f(\nabla u) = -\nabla \cdot \left(\frac{\nabla u}{1+|\nabla u|^2} \right)$ and correspondingly $F(\nabla u) = -\frac{1}{2} \ln(|\nabla u|^2 + 1)$;
- the phase field crystal equation, $G = \Delta$, $\mathcal{L} = (\Delta+1)^2$, $f(u) = u^3 - \epsilon u$ and $F(u) = \frac{1}{4}(u^2 - \epsilon)^2$.

We shall assume that f is a Lipschitz continuous function with the Lipschitz constant β , i.e. we have

$$\|f(u) - f(v)\| \leq \beta\|u - v\|, \quad \forall u, v \in \mathcal{H}. \quad (2.4)$$

This may appear to be somewhat restrictive since $f(u)$ in some popular phase-field models, such as Allen-Cahn, Cahn-Hilliard and phase field crystal, does not naturally satisfy the above Lipschitz assumption. However, as long as exact solutions of the problem in consideration are uniformly bounded, which is true for a large class of phase-field models, we can truncate $f(u)$ to quadratic growth as in [28, 11] so as to satisfy the Lipschitz assumption. In practice such modification does not affect convergence because of the boundedness of their solutions (cf. [21, 22], which offer solid analysis).

Note that for the MBE model, the functions F and f are of ∇u , which is different from other examples. The Lipschitz condition is satisfied in the sense

$$\|\partial_{\nabla u}^2 F(\nabla u)\|_2 \leq 1, \quad (2.5)$$

which also bounds the growth of the nonlinear term.

Consider the natural splitting of the energy $E(u) = E_l - E_n$ with

$$\begin{aligned} E_l(u) &= \int_{\Omega} \left(\frac{1}{2} |\mathcal{L}_{1/2} u|^2 + \frac{\beta}{2} |u|^2 \right) dx, \\ E_n(u) &= \int_{\Omega} \left(F(u) + \frac{\beta}{2} |u|^2 \right) dx. \end{aligned} \quad (2.6)$$

From this perspective, the gradient flow can thus be written as

$$u_t = G(Lu - g(u)), \quad (2.7)$$

where $L = \beta I + \mathcal{L}$ and $g = \beta I - f$ correspond to E_l and E_n respectively. In the computation, Lu is treated implicitly and $g(u)$ is treated explicitly, which leads to linearly implicit schemes.

Here β serves as a stabilization to enhance the dissipation of linear part, so as to bound the Lipschitz growing nonlinear term in the analysis. In fact, such modification or stabilization is necessary for the proof of energy decay, which is pointed out in the remark attached to the main theorem. However, the stabilization may cause significant time delay phenomena if a low-order scheme is used or a large time step is taken. We will study the effect in detail for higher-order schemes in Section 4. On the other hand, the stabilization is necessary to guarantee the MBP for Allen-Cahn equations [6]. Besides, [26] provides numerical evidences to illustrate that the stabilization can improve the numerical performance significantly.

2.2 ETDRK methods

The key idea of ETDRK is to consider Duhamel's principle for the equation (2.7)

$$u(x, t) = e^{GL(t-t_0)} u(x, t_0) - e^{GL(t-t_0)} \int_{t_0}^t e^{-GL(s-t_0)} Gg(u(x, s)) ds, \quad (2.8)$$

and approximate the implicit integral with a suitable quadrature formula. For example, assuming that we have u_n , the approximate solution at time step n , the simplest way to determine u_{n+1} is

to substitute the function $g(u)$ by a constant $g(u_n)$ which leads to the first-order ETD (ETD1) scheme:

$$u_{n+1} = e^{\tau GL} u_n + (I - e^{\tau GL}) L^{-1} g(u_n), \quad (2.9)$$

where τ is the time step. For this scheme, the energy dissipation law and MBP for the Allen-Cahn equation particularly have been proved, see, e.g. [7]. The classical second order ETDRK (ETDRK2) for the gradient flow (1.1) reads

$$v = e^{\tau GL} u_n + (I - e^{\tau GL}) L^{-1} g(u_n), \quad (2.10)$$

$$u_{n+1} = v - \frac{1}{\tau} (e^{\tau GL} - I - \tau GL) (GL)^{-2} (Gg(v) - Gg(u_n)). \quad (2.11)$$

It is shown in [11] that the above scheme is energy decreasing with a suitably large stabilization constant β for the Allen-Cahn and Cahn-Hilliard equations.

In general, the ETDRK schemes take the following form [5]:

$$\begin{aligned} v_1 &= u_n, \\ v_i &= \chi_i(\tau GL) u_n - \tau \sum_{j=1}^{i-1} a_{ij}(\tau GL) Gg(v_j), \quad i = 2, \dots, s, \\ u_{n+1} &= \chi(\tau GL) u_n - \sum_{j=1}^s b_j(\tau GL) Gg(v_j), \end{aligned} \quad (2.12)$$

where $\chi(z) = e^z$, $\chi_i(z) = \chi(c_i z)$, and the coefficients a_{ij}, b_j are constructed to equal to or approximate exponential functions. For simplicity we define a class of functions which will be frequently used

$$\phi_0(z) = e^z, \quad \phi_{k+1}(z) = \frac{\phi_k(z) - \phi_k(0)}{z}, \quad \text{with } \phi_k(0) = 1/k!. \quad (2.13)$$

The ETDRK schemes (2.12) could also be written in Butcher Tableau, although now its coefficients are functions

$$\begin{array}{c|ccc|c} c_1 & & & & \chi_1(\tau GL) \\ c_2 & a_{21} & & & \chi_2(\tau GL) \\ \dots & \dots & \dots & & \dots \\ c_s & a_{s1} & \dots & a_{s,s-1} & \chi_s(\tau GL) \\ \hline & b_1 & b_2 & \dots & b_s & \chi(\tau GL) \end{array} \quad (2.14)$$

In order to preserve the equilibria, the coefficients of the method have to satisfy

$$\sum_{j=1}^s b_j(z) = \frac{\chi(z) - 1}{z}, \quad \sum_{j=1}^s a_{ij}(z) = \frac{\chi_i(z) - 1}{z}. \quad (2.15)$$

Taking the ETDRK2 as an example, $a_{21}(z) = \phi_1(z) = (e^z - 1)/z$, $b_2(z) = \phi_2(z) = (e^z - z - 1)/z^2$ and $b_1 = \phi_1 - \phi_2$, where $z = \tau GL$ and its Butcher Tableau reads

$$\begin{array}{c|cc|c} 0 & & & 1 \\ 1 & \phi_1(\tau GL) & & \chi(\tau GL) \\ \hline & \phi_1(\tau GL) - \phi_2(\tau GL) & \phi_2(\tau GL) & \chi(\tau GL) \end{array} \quad (2.16)$$

With the help of (2.15) and setting $u_{n+1} = v_{s+1}$, we can rewrite the solution (2.12) as

$$\begin{aligned} v_i &= u_n + \tau \sum_{j=1}^{i-1} a_{ij}(\tau GL)(GLu_n - Gg(v_j)), \quad i = 2, \dots, s, \\ v_{s+1} &= u_n + \tau \sum_{j=1}^s b_j(\tau GL)(GLu_n - Gg(v_j)). \end{aligned} \quad (2.17)$$

2.3 A general framework for energy stable ETDRK schemes

We present below a general framework for constructing energy stable ETDRK schemes. We start with a useful lemma whose proof is straightforward.

Lemma 2.1. *Consider a positive-definite operator $L = \beta I + \mathcal{L}$, and let f be an analytic function whose domain includes the spectrum of L , i.e. the values $\{f(\lambda_i)\}_{i \in \mathcal{N}}$ exist, where $\{\lambda_i\}_{i \in \mathcal{N}}$ are the eigenvalues of L . Then, the eigenvalues of $f(L)$ are $\{f(\lambda_i)\}_{i \in \mathcal{N}}$. Furthermore, if f is a positive function, then $f(L)$ is also a positive-definite operator.*

Hereafter, we say a matrix Δ is positive-definite if the eigenvalues of its symmetrizer $(\Delta + \Delta^T)/2$ are all positive. The main result of this paper is stated below.

Theorem 2.1. *Consider the gradient flow*

$$u_t = G(\mathcal{L}u + f(u)), \quad (x, t) \in \Omega \times [0, T] \quad (2.18)$$

where G is a negative operator, \mathcal{L} is a sectorial operator and f is a Lipschitz continuous function with the Lipschitz constant β . The ETDRK schemes (2.12) unconditionally decreases the energy as long as the following determinant

$$\Delta(z) = zE_L + P^{-1}E_L - \frac{z}{2}I, \quad (2.19)$$

is positive-definite for all negative $z \in \mathbb{R}$, where I is the identity operator, $E_L = (1_{i \geq j})_{s \times s}$ is the lower triangular matrix with all nonzero entries equal to 1, and

$$P = \begin{pmatrix} a_{21} & & & & & \\ a_{31} & a_{32} & & & & \\ \vdots & \vdots & \ddots & & & \\ a_{s1} & a_{s2} & \cdots & a_{s(s-1)} & & \\ b_1 & b_2 & \cdots & b_{s-1} & b_s & \end{pmatrix}, \quad (2.20)$$

where a_{ij} and b_i are given in (2.14).

Proof. We first compute the difference of the energy and derive a key inequality.

Since the function f is Lipschitz continuous, given any v, u , we have

$$\begin{aligned} (F(v) - F(u), 1) &\leq (v - u, f(u)) + \frac{\beta}{2}(v - u, v - u) \\ &= -(v - u, g(u)) + \beta(v - u, u) + \frac{\beta}{2}(v - u, v - u). \end{aligned} \quad (2.21)$$

On the other hand,

$$\begin{aligned}
\frac{1}{2} \left(\int_{\Omega} |\mathcal{L}_{1/2} v|^2 - |\mathcal{L}_{1/2} u|^2 dx \right) &= \frac{1}{2} ((v, \mathcal{L}v) - (u, \mathcal{L}u)) \\
&= (v - u, \mathcal{L}v) - \frac{1}{2} (v - u, \mathcal{L}(v - u)) \\
&= (v - u, Lv) - \beta(v - u, v) - \frac{1}{2} (v - u, \mathcal{L}(v - u)),
\end{aligned} \tag{2.22}$$

where we used the identity

$$[a, a] - [b, b] = 2[a - b, a] - [a - b, a - b]$$

which is valid for all a, b and any bilinear form $[\cdot, \cdot]$. Therefore, combining these two parts we derive

$$\begin{aligned}
E(v) - E(u) &\leq (v - u, Lv - g(u)) - \beta(v - u, v - u) - \frac{1}{2} (v - u, \mathcal{L}(v - u)) \\
&\leq (v - u, Lv - g(u)) - \frac{1}{2} (v - u, (\beta I + L)(v - u)).
\end{aligned} \tag{2.23}$$

This vital inequality holds with the Lipschitz condition.

Now we focus on the ETDRK scheme (2.17), the first line of which is $v_1 = u_n$, and the rest can be rewritten as the following system

$$\begin{pmatrix} v_2 - v_1 \\ v_3 - v_1 \\ \dots \\ v_{s+1} - v_1 \end{pmatrix} = \tau P \begin{pmatrix} G(Lv_1 - g(v_1)) \\ G(Lv_1 - g(v_2)) \\ \dots \\ G(Lv_1 - g(v_s)) \end{pmatrix}, \tag{2.24}$$

which is equivalent to

$$\begin{pmatrix} Lv_1 - g(v_1) \\ Lv_1 - g(v_2) \\ \dots \\ Lv_1 - g(v_s) \end{pmatrix} = \frac{1}{\tau} P^{-1} \begin{pmatrix} G^{-1}(v_2 - v_1) \\ G^{-1}(v_3 - v_1) \\ \dots \\ G^{-1}(v_{s+1} - v_1) \end{pmatrix} = \frac{1}{\tau} P^{-1} E_L \begin{pmatrix} G^{-1}(v_2 - v_1) \\ G^{-1}(v_3 - v_2) \\ \dots \\ G^{-1}(v_{s+1} - v_s) \end{pmatrix}. \tag{2.25}$$

Therefore,

$$\begin{aligned}
E(u_{n+1}) - E(u_n) &= \sum_{k=1}^s E(v_{k+1}) - E(v_k) \\
&\leq \sum_{k=1}^s (v_{k+1} - v_k, Lv_{k+1} - g(v_k)) - \frac{1}{2} \sum_{k=1}^s (v_{k+1} - v_k, (\beta I + L)(v_{k+1} - v_k)) \\
&= \sum_{k=1}^s ((v_{k+1} - v_k, Lv_{k+1} - Lv_1) + (v_{k+1} - v_k, Lv_1 - g(v_k))) \\
&\quad - \frac{1}{2} \sum_{k=1}^s (v_{k+1} - v_k, (\beta I + L)(v_{k+1} - v_k)) \quad (\text{using (2.25)}) \\
&= \frac{1}{\tau} \sum_{k=1}^s \sum_{j=1}^k (v_{k+1} - v_k, G^{-1}(\tau GL)(v_{j+1} - v_j)) + (v_{k+1} - v_k, G^{-1}(P^{-1}E_L)_{kj}(v_{j+1} - v_j)) \\
&\quad - \frac{\beta}{2} \sum_{k=1}^s (v_{k+1} - v_k, v_{k+1} - v_k) - \frac{1}{2\tau} \sum_{k=1}^s (v_{k+1} - v_k, G^{-1}(\tau GL)(v_{k+1} - v_k)) \\
&= \frac{1}{\tau} \sum_{k,j=1}^s (v_{k+1} - v_k, G^{-1}\Delta_{kj}(\tau GL)(v_{j+1} - v_j)) - \frac{\beta}{2} \sum_{k=1}^s (v_{k+1} - v_k, v_{k+1} - v_k),
\end{aligned} \tag{2.26}$$

where $\Delta(z) = zE_L + P^{-1}E_L - \frac{z}{2}I$ with $z = \tau GL$. Since the last term in the above is negative, and G is a negative operator, we find that the discrete energy unconditionally decreases if $\Delta(z)$ is positive-definite for all negative $z \in R$. \square

Remark 2.1. For the MBE model, recall that the nonlinear term is Lipschitz continuous as a function of ∇u , and meanwhile the convex splitting of the energy is also different (Or see [33, 20] for more details), but all analysis in the proof can be carried out in the similar way. To keep the presentation short, we omit the proof.

Remark 2.2. The inequality (2.23) in the proof plays a very important role. It is the only place where we apply the Lipschitz condition. Alternatively, we can also replace the Lipschitz condition by a convex splitting approach since

$$\begin{aligned}
E(v) - E(u) &\leq \left(v - u, \frac{\delta E_l}{\delta v}(v) - \frac{\delta E_n}{\delta u}(u) \right) \\
&= (v - u, Lv + f(u)) \\
&= (v - u, Lv - g(u)) - \beta(v - u, v - u).
\end{aligned} \tag{2.27}$$

The determinant of this version is slightly different but the rest of proof is the same.

Lemma 2.2. The positive-definiteness of $\frac{1}{2}(\Delta + \Delta^T)$ is the same as the positive-definiteness of

$$\Delta' = zPEP^T + E_L P^T + PE_L^T.$$

Proof. Notice that

$$E_L + E_L^T = E + I,$$

and

$$P(\Delta + \Delta^T)P^T = P(E_L + E_L^T - I)P^T + E_L P^T + P E_L^T = \Delta'.$$

□

Remark 2.3. Δ' is already symmetric and helps us in the understanding and subsequent proof regarding the positive-definiteness.

3 Examples of energy decreasing ETDRK schemes

In this section we consider some examples of ETDRK methods up to order four.

We first recall

$$\phi_0(z) = e^z, \quad \phi_{k+1} = \frac{\phi_k(z) - \phi_k(0)}{z}, \quad \phi_k(0) = 1/k! \quad (3.1)$$

We will also denote $\phi_{i,j}(z) = \phi_i(c_j z)$ for simplicity.

3.1 First-order ETD scheme

We start with the very simple ETD1 scheme

$$u_{n+1} = e^{\tau GL} u_n + (I - e^{\tau GL}) L^{-1} g(u_n), \quad (3.2)$$

whose Butcher Tableau reads

$$\begin{array}{c|c} 0 & 0 \\ \hline & \phi_1(\tau GL) \end{array}. \quad (3.3)$$

Corollary 3.1. *The first-order ETD scheme unconditionally decreases the discrete energy.*

Proof. The only element in P is $b_1 = \phi_1$, whence the determinant $\Delta = z + 1/\phi_1(z) - z/2 = ze^z/(e^z - 1) - z/2$. Therefore, $\Delta \geq 0$ always holds for $z \leq 0$. The theorem (2.1) guarantees that the discrete energy of the ETD1 solution unconditionally decreases. □

3.2 Second-order ETDRK scheme

In [11] it has been proven that the following ETDRK2 scheme is unconditionally energy stable, while here we could make use of the framework to obtain the same result. In fact, the estimate here is finer than the result in [11].

We consider the following ETDRK2 scheme

$$v = e^{\tau GL} u_n + (I - e^{\tau GL}) L^{-1} g(u_n), \quad (3.4)$$

$$u_{n+1} = v - \frac{1}{\tau} (e^{\tau GL} - I - \tau GL) (GL)^{-2} (Gg(v) - Gg(u_n)). \quad (3.5)$$

The Butcher Tableau reads

$$\begin{array}{c|cc} 0 & 0 & \\ 1 & \phi_1 & \\ \hline & \phi_1 - \phi_2 & \phi_2 \end{array}. \quad (3.6)$$

Corollary 3.2. *The second-order ETDRK scheme unconditionally decreases the discrete energy.*

Proof. According to the Butcher Tableau, we have

$$P = \begin{pmatrix} \phi_1 & 0 \\ \phi_1 - \phi_2 & \phi_2 \end{pmatrix}, \quad P^{-1} = \begin{pmatrix} 1/\phi_1 & 0 \\ (\phi_2 - \phi_1)/(\phi_1\phi_2) & 1/\phi_2 \end{pmatrix},$$

whence the determinant reads

$$\Delta = \begin{pmatrix} z + 1/\phi_1 & 0 \\ z + 1/\phi_1 & z + 1/\phi_2 \end{pmatrix} - \frac{z}{2}I_2 = (z + 1/\phi_1)E_L + \begin{pmatrix} 0 & 0 \\ 0 & 1/\phi_2 - 1/\phi_1 \end{pmatrix} - \frac{z}{2}I_2. \quad (3.7)$$

The first term is positive-definite since $(z + 1/\phi_1)$ is positive and E_L is positive-definite, the second term is also positive-definite because $\phi_1 > \phi_2 > 0$, and the third term is obviously positive-definite. Therefore, Δ is positive-definite and the ETDRK2 scheme is unconditionally energy stable. \square

3.3 Third-order ETDRK schemes

In general, third-order ETDRK schemes need to satisfy the following order conditions:

Order	Conditions
1	$\psi_1 = 0$
2	$\psi_2 = 0$
2	$\psi_{1,i} = 0$
3	$\psi_3 = 0$
3	$\sum_{i=1}^s b_i J \psi_{2,i} = 0$

where

$$\psi_i(z) = \phi_i(z) - \sum_{k=1}^s b_k c_k^{j-1} / (j-1)!, \quad \psi_{i,j} = \phi_i c_j^i - \sum_{k=1}^{j-1} a_{jk} c_k^{i-1} / (i-1)!, \quad (3.8)$$

and J denotes arbitrary bounded operators. In particular, the classical ETDRK3 scheme below from Cox and Mathews [5] does not satisfy the conditions of our theorem (see Fig. 2) so it is not unconditionally energy decreasing.

$$\begin{array}{c|ccc} 0 & & & \\ \frac{1}{2} & \frac{1}{2}\phi_{1,2} & & \\ 1 & -\phi_{1,3} & 2\phi_{1,3} & \\ \hline & 4\phi_3 - 3\phi_2 + \phi_1 & -8\phi_3 + 4\phi_2 & 4\phi_3 - \phi_2 \end{array} \quad (3.9)$$

On the other hand, all possible types of three-stage third-order ETDRK schemes are listed in [14, 15]. In fact, many of them with suitable coefficients could satisfy the requirement of our theorem, and two of them are described with the Butcher Tableaux below:

$$\begin{array}{c|ccc} 0 & & & \\ 1 & \phi_1 & & \\ \frac{2}{3} & \frac{2}{3}\phi_{1,3} - \frac{4}{9}\phi_{2,3} & \frac{4}{9}\phi_{2,3} & \\ \hline & \frac{3}{4}\phi_1 - \phi_2 & \phi_2 - \frac{1}{2}\phi_1 & \frac{3}{4}\phi_1 \end{array} \quad (3.10)$$

and

$$\begin{array}{c|ccc} 0 & & & \\ \frac{4}{9} & \frac{4}{9}\phi_{1,2} & & \\ \frac{2}{3} & \frac{2}{3}\phi_{1,3} - \phi_{2,3} & \phi_{2,3} & \\ \hline \frac{2}{3} & \phi_1 - \frac{3}{2}\phi_2 & 0 & \frac{3}{2}\phi_2 \end{array} \quad (3.11)$$

To begin with, we first present numerical evidences. We plot in Fig. 2 the smallest eigenvalues of $\frac{1}{2}(\Delta + \Delta^T)$ for the three schemes above, and we observe that the smallest eigenvalues of (3.10) and (3.11) are positive, indicating that the conditions of our theorem are satisfied, while the smallest eigenvalues for the scheme (3.9) when Z approaches zero become negative, which indicates that the conditions of our theorem are violated. To rigorously show that the above two ETDRK schemes decrease the energy, we only need to prove the positive-definiteness of Δ' for the above schemes, which could be verified by checking all leading principal minors.

Proposition 3.1. *For the schemes (3.10) and (3.11), the determinants of all leading principal minors of Δ' are positive, and thus Δ' is positive definite. Thus, the schemes (3.10) and (3.11) unconditionally decrease the energy for general gradient flows (2.7).*

Proof. According to (3.10), we derive the expressions for determinants of leading principal minors

$$\begin{aligned} \text{Det}(\Delta'_{1 \times 1}) &= \Delta'_{11} = \frac{e^z - 1}{z} > 0; \\ \text{Det}(\Delta'_{2 \times 2}) &= \frac{1}{9z^4}(-9e^{4z/3} + 18e^{2z/3} + 6z - 6ze^{2z/3} - 18ze^{5z/3} + 18ze^{7z/3} - 9z^2e^{2z} - 9z^2e^{4z/3} \\ &\quad + 6z^2e^{5z/3} + 8z^2 - 9); \\ \text{Det}(\Delta') &= \frac{1}{36z^6}(252z + 162e^{2z} - 162e^{2z/3} + 324e^{5z/3} - 162e^{8z/3} - 324e^z + 99ze^{2z} + 54ze^{3z} \\ &\quad - 81ze^{4z} - 180ze^{2z/3} - 45ze^{4z/3} + 378ze^{5z/3} + 54ze^{7z/3} - 468ze^{8z/3} - 9ze^{10z/3} \\ &\quad + 270ze^{11z/3} - 72z^2e^z + 78z^2e^{2z} - 18z^2e^{3z} + 83z^3e^{2z} + 6z^2e^{2z/3} - 54z^2e^{4z/3} \\ &\quad + 288z^2e^{5z/3} + 27z^3e^{4z/3} + 18z^3e^{5z/3} - 54z^2e^{7z/3} - 240z^2e^{8z/3} - 324ze^z + 66z^2 \\ &\quad - 20z^3 + 162). \end{aligned}$$

It can be verified by Fig. 1 that for z with small absolute values,

$$\begin{aligned} z^4 \text{Det}(\Delta'_{2 \times 2}) &\geq 0.2, \quad z \in [-3, -1], & \text{Det}(\Delta'_{2 \times 2}) &\geq 0.2, \quad \forall z \in [-1, 0), \\ z^6 \text{Det}(\Delta') &\geq 0.1, \quad z \in [-6, -1], & \text{Det}(\Delta') &\geq 0.1, \quad \forall z \in [-1, 0), \end{aligned}$$

where both $z^4 \text{Det}(\Delta')_{2 \times 2}$ and $z^6 \text{Det}(\Delta')$ are smooth decreasing functions and both $\text{Det}(\Delta')_{2 \times 2}$ and $\text{Det}(\Delta')$ are smooth increasing functions.

For z with large scales, we use the non-exponential term to control the exponentially small term. Therefore, we denote the non-exponential term in $z^4 \text{Det}(\Delta'_{2 \times 2})$ as

$$P_2 = (6z + 8z^2 - 9)/9$$

and the exponential term as

$$R_2 = (-9e^{4z/3} + 18e^{2z/3} - 6ze^{2z/3} - 18ze^{5z/3} + 18ze^{7z/3} - 9z^2e^{2z} - 9z^2e^{4z/3} + 6z^2e^{5z/3})/9.$$

When $z < -3$,

$$P_2(z) > P_2(-3) = 6,$$

$$|R_2| < (9e^{-4} + 18e^{-2} + 6 \times 3e^{-2} + 18 \times 3e^{-5} + 18 \times 3e^{-7} + 9 \times 3^2e^{-2} + 9 \times 3^2e^{-4} + 6 \times 3^2e^{-5})/9 < 2.03,$$

where we use $\beta \leq |\beta|$ for every single term in R_2 . Thus, $z^4 \text{Det}(\Delta'_{2 \times 2}) \geq P_2 - |R_2| > 6 - 2.03 > 0$ for all $z < -3$.

Similarly we could define the non-exponential term P_3 and the exponential term R_3 for $z^6 \text{Det}(\Delta)$, and for $z < -6$, we have $P_3(z) > P_3(-6) = 148.5$, $|R_3(z)| < 86$ and thus $z^6 \text{Det}(\Delta') > P_3(z) - |R_3(z)| > 0$. Combine all above results, we have $\text{Det}(\Delta'_{2 \times 2}) > 0$, and $\text{Det}(\Delta') > 0$ for all negative z .

Therefore, all the determinants of leading principal minors are positive, i.e. Δ' is positive-definite.

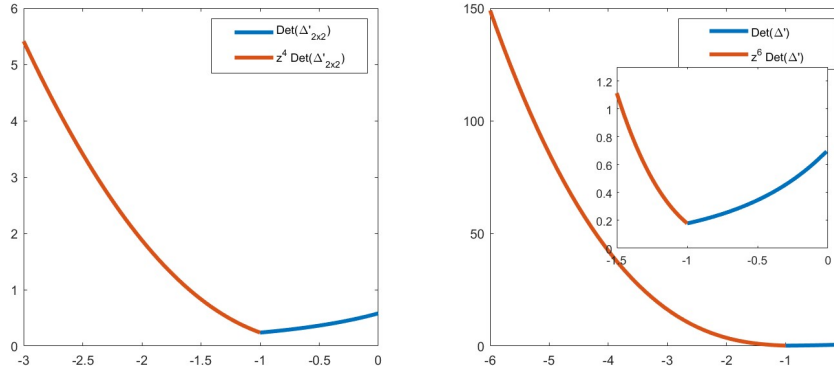


Figure 1: Positive-definiteness test: Determinants of leading principal minors

For the scheme (3.11), the proof is the same and we just present the determinants of leading principal minors here.

$$\begin{aligned} \text{Det}(\Delta'_{1 \times 1}) &= \Delta'_{11} = \frac{e^{8z/9} - 1}{z} > 0; & \text{Det}(\Delta'_{2 \times 2}) &= -\frac{1}{16z^4} (36z - 162e^{2z/3} + 81e^{4z/3} - 36ze^{2z/3} \\ &+ 72ze^{10z/9} - 72ze^{16z/9} + 16z^2e^{4z/3} + 16z^2e^{8z/9} + 16z^2e^{10z/9} - 12z^2 + 81); \\ \text{Det}(\Delta') &= -\frac{1}{32z^5} (22e^{2z} - 71z + 288e^{2z/3} - 130e^{4z/3} - 216e^{5z/3} + 80e^{7z/3} - 72e^{8z/3} + 50e^{10z/3} \\ &+ 136e^z + 5ze^{2z} + 63ze^{2z/3} + 16ze^{4z/3} - 86ze^{5z/3} + 4ze^{7z/3} + 23ze^{8z/3} - 20ze^{10z/3} \\ &- 128ze^{10z/9} - 28ze^{13z/9} + 144ze^{16z/9} - 4ze^{19z/9} + 172ze^{22z/9} - 156ze^{28z/9} - 4z^2e^z \\ &- 50z^2e^{2z} - 30z^2e^{4z/3} + 8z^2e^{5z/3} - 4z^2e^{7z/3} + 56z^2e^{8z/3} + 2z^2e^{10z/3} - 30z^2e^{8z/9} \\ &- 28z^2e^{10z/9} - 8z^2e^{13z/9} + 12z^2e^{17z/9} + 8z^2e^{19z/9} + 40z^2e^{22z/9} + 18z^2e^{26z/9} \\ &- 12z^2e^{28z/9} + 66ze^z + 22z^2 - 158). \end{aligned}$$

□

Since the scheme (3.10) has the largest positive smallest eigenvalue according to the following Fig. 2, we shall use it to represent energy stable ETDRK3 for numerical tests in Section 4.

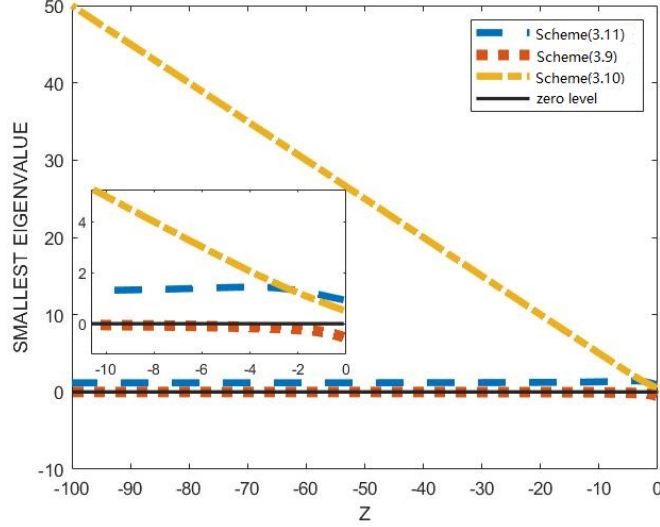


Figure 2: Eigenvalues of $\frac{1}{2}(\Delta + \Delta^T)$ for the three ETDRK3 schemes

3.4 Fourth-order ETDRK schemes

In general, fourth-order ETDRK schemes need to satisfy four more order conditions:

Order	Conditions
4	$\psi_4 = 0$
4	$\sum_{i=1}^s b_i J \psi_{3,i} = 0$
4	$\sum_{i=1}^s b_i J \sum_{j=2}^{i-1} a_{ij} J \psi_{2,j} = 0$
4	$\sum_{i=1}^s b_i c_i K \psi_{2,i} = 0$

where $\psi_i(z) = \phi_i(z) - \sum_{k=1}^s b_k c_k^{j-1} / (j-1)!$, $\psi_{i,j} = \phi_i c_j^i - \sum_{k=1}^{j-1} a_{jk} c_k^{i-1} / (i-1)!$, and J, K denote arbitrary bounded operators (for more details, see [15]). These fourth-order conditions are more complicated than previous third-order conditions so that it is more difficult to construct fourth-order ETDRK schemes. One of the most used ETDRK4 schemes is from Cox and Mathews [5]:

$$\begin{array}{c|cccc}
 0 & & & & \\
 \frac{1}{2} & \frac{1}{2}\phi_{1,2} & & & \\
 \frac{1}{2} & 0 & \frac{1}{2}\phi_{1,3} & & \\
 1 & \frac{1}{2}\phi_{1,3}(\phi_{0,3} - 1) & 0 & \phi_{1,3} & \\
 \hline
 & \phi_1 - 3\phi_2 + 4\phi_3 & 2\phi_2 - 4\phi_3 & 2\phi_2 - 4\phi_3 & 4\phi_3 - \phi_2
 \end{array} \tag{3.12}$$

The other is given by Krogstad [19]:

$$\begin{array}{c|cccc}
 0 & & & & \\
 \frac{1}{2} & \frac{1}{2}\phi_{1,2} & & & \\
 \frac{1}{2} & \frac{1}{2}\phi_{1,3} - \phi_{2,3} & \phi_{2,3} & & \\
 1 & \phi_{1,4} - 2\phi_{2,4} & 0 & 2\phi_{2,4} & \\
 \hline
 & \phi_1 - 3\phi_2 + 4\phi_3 & 2\phi_2 - 4\phi_3 & 2\phi_2 - 4\phi_3 & 4\phi_3 - \phi_2
 \end{array} \tag{3.13}$$

We plot in Fig. 3 the smallest eigenvalues of $\frac{1}{2}(\Delta + \Delta^T)$ for the above two schemes, the results clearly indicate that the above two schemes do not satisfy our conditions for energy stability. Moreover, we checked all existing fourth-order ETDRK schemes that we could find, and also

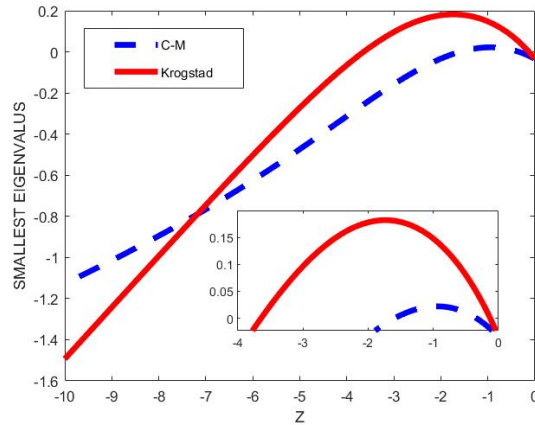


Figure 3: Eigenvalues of ETDRK4 schemes from Cox and Mathhews [5], and Krogstad [19]

tried to search from a wide family of four-stage and five-stage fourth-order ETDRK methods, but none of them satisfy the requirement of our theorem. Therefore, the existence of energy stable ETDRK4 schemes is still an open problem.

4 Numerical Experiments

In this section we carry out some numerical experiments to illustrate the convergence and energy decay property of ETDRK schemes for different phase-field models. We first verify the temporal convergence rates with smooth initial data for the Allen–Cahn and Cahn–Hilliard equations. Next we study the large time step behavior for the Allen–Cahn, Cahn–Hilliard and phase field crystal equations. Then we present energy curves with different time steps and stabilization constants to observe their influence. Finally we present an adaptive time stepping example which makes full use of the unconditional energy stability.

In all simulations, we consider models with periodic conditions, and use a Fourier-spectral method in space with a sufficiently fine mesh so that the spatial discretization errors can be ignored compared with temporal discretization errors. The ETDRK3 scheme (3.10) is used if not specified otherwise. Besides, we also consider a truncated double-well potential $\tilde{F}(u)$ so that

it naturally satisfies the Lipschitz condition. More precisely, for a sufficiently large M ($M = 2$ is enough for cases in this paper), we replace $F(u) = \frac{1}{4}(u^2 - 1)^2$ by

$$\tilde{F}(u) = \begin{cases} \frac{3M^2 - 1}{2}u^2 - 2\text{sgn}(u)M^3u + \frac{1}{4}(3M^4 + 1), & |u| > M \\ \frac{1}{4}(u^2 - 1)^2, & |u| \leq M \end{cases},$$

and $f(u) = u^3 - u$ by

$$\tilde{f}(u) = \tilde{F}'(u) = \begin{cases} (3M^2 - 1)u - 2\text{sgn}(u)M^3, & |u| > M \\ u^3 - u, & |u| \leq M \end{cases}.$$

In fact, the maximum norm of numerical solutions never exceeds the bound M so this replacement does not affect the properties of numerical solutions.

4.1 Convergence tests

We solve the Allen–Cahn and Cahn–Hilliard equations in $\Omega = (0, 2\pi) \times (0, 2\pi)$ with the smooth initial data $u_0 = 0.5 \sin x \sin y$. To compute the errors and the convergence rate, we take the number of grid points $N = 128$, the interfacial parameter $\epsilon = 0.5$ and set the final time $T = 0.32$. With these settings we compute the numerical solutions with various time steps $\tau = 0.01/2^k$ with $k = 0, 1, \dots, 4$ and calculate the relative errors to get the convergence rate. The results for the Allen-Cahn and Cahn-Hilliard equations are listed in Tables 1 and 2, respectively. In both cases, desired convergence rates are observed.

$\tau=0.01$	L^∞ err	rate	L^2 err	rate
τ	2.6852e-08	-	2.0736e-09	-
$\tau/2$	3.4044e-09	2.9795	2.6291e-10	2.9795
$\tau/4$	4.2863e-10	2.9896	3.3101e-11	2.9896
$\tau/8$	5.3815e-11	2.9936	4.1557e-12	2.9937
$\tau/16$	6.7815e-12	2.9883	5.2341e-13	2.9891

Table 1: ETDRK3 errors and convergence rates for the Allen-Cahn equation

$\tau=0.01$	L^∞ err	rate	L^2 err	rate
τ	4.2646e-07	-	3.7881e-08	-
$\tau/2$	5.3484e-08	2.9952	4.8765e-09	2.9576
$\tau/4$	6.6767e-09	3.0019	6.1872e-10	2.9785
$\tau/8$	8.3316e-10	3.0025	7.7913e-11	2.9894
$\tau/16$	1.0392e-10	3.0032	9.7637e-12	2.9964

Table 2: ETDRK3 errors and convergence rates for the Cahn-Hilliard equation

4.2 Large time step tests

In this subsection we study the accuracy of solutions with large time steps. We set $N = 128$, $T = 8$, $\epsilon = 0.1$ for the Allen–Cahn equation and $\epsilon = 0.5$ for the Cahn–Hilliard equation and

observe the relation between the error and the time steps $\tau = 2^{1-k}, k = 0, 1, \dots, 7$ in Fig. 4. We could see that with large time steps the solutions still have good performances.

We also simulated the phase field crystal model with $N = 256$, $\epsilon = 0.025$ and $\beta = 3$ in $\Omega = (0, 32) \times (0, 32)$. We use both ETDRK2 and ETDRK3 to solve it with the initial condition $u_0 = \sin(\frac{\pi x}{16}) \sin(\frac{\pi y}{16})$, and computed the solution at $T = 1$ with $\tau = 2^{-k}, k = 0, 1, \dots, 11$. The results are plotted in Fig. 5. We observe that both ETDRK schemes performed well with large time steps. More precisely, with $\tau = 0.1$, the errors of ETDRK3 and ETDRK2 are about $O(10^{-4})$ and $O(10^{-3})$, respectively.

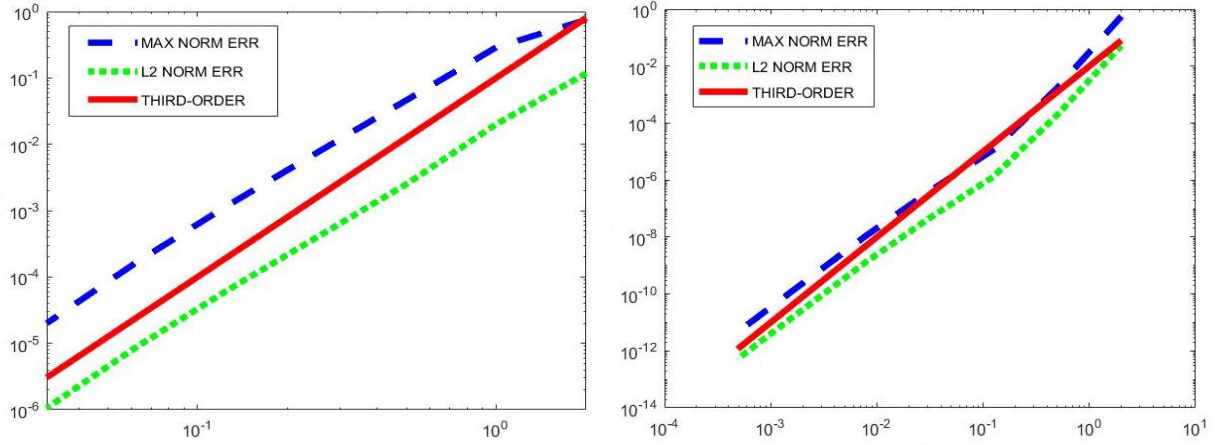


Figure 4: Error- τ figure for the AC (left) and CH (right)

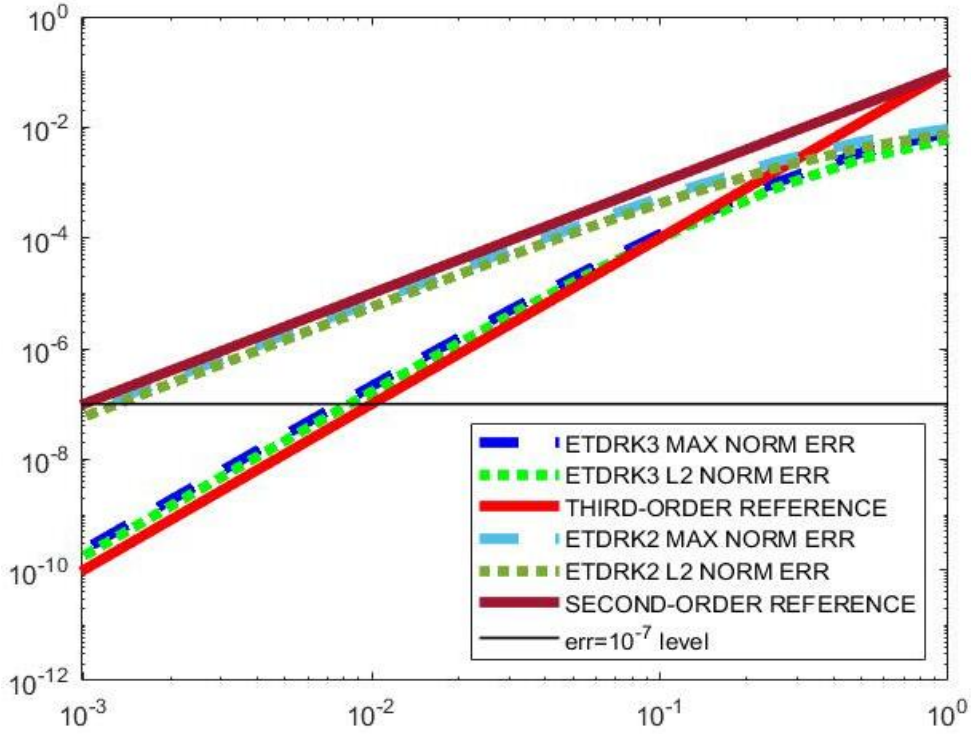


Figure 5: Error- τ figure for the phase-field crystal model

4.3 Energy curves with different time steps and stabilization constants

Now we study how energy curves behave with different time steps and stabilization constants. It is well-known that stabilization may affect the dynamics and cause serious time delay phenomena when lower-order schemes are used or large time steps are taken. We first test the Cahn–Hilliard equation with $N = 128$, $\epsilon = 0.1$ and $\beta = 2$. The results are presented in Fig. 6. We observe that when time steps are large, the time delay phenomena is obvious, while when $\tau \leq 0.01$, the influence becomes negligible.

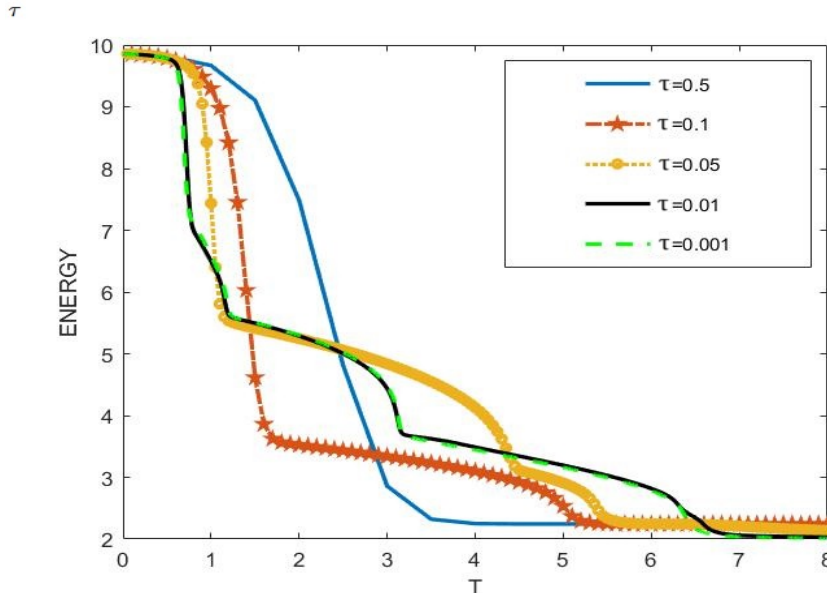


Figure 6: Energy curves with different time steps for the Cahn-Hilliard equation

Next we examine the effect of different stabilization constants. Although theoretically they have to be larger than the Lipschitz constant, we could still run the simulation with smaller stabilization constants. While smaller stabilization constants cause less time delay, but solutions may lose its accuracy and even blow-up. Fig.7 shows that when $\tau = 0.1$, the solutions are all inaccurate and have obvious time delay, and the solution with $\beta = 0.1$ even has unwanted oscillations. This evidence indicates that the stabilization does help the numerical solutions to maintain stability. When $\tau = 0.01$, all three curves with $\beta = 0.1, 1, 2$ are very close, which indicates that the stabilization does not affect much when the time step is small.

4.4 Long time behavior of the phase field crystal model

Next, we simulate the long time evolution of the phase field crystal (PFC) model with $N = 256$, $\epsilon = 0.025$, $\Omega = (0, 128) \times (0, 128)$, and the initial condition

$$u_0 = 0.05 + 0.01 * rand(x), \quad x \in \Omega \quad (4.1)$$

where $rand(x)$ is a uniformly distributed random function satisfying $-1 \leq rand(x) \leq 1$. The long time behavior of the solution obtained by ETDRK3 with $\beta = 3$ and $\tau = 0.1$ is presented in Fig.8.

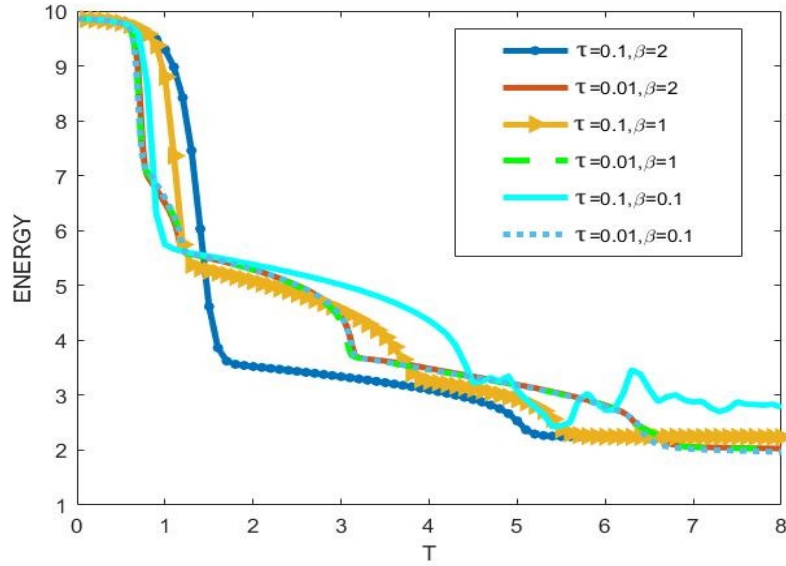


Figure 7: Energy curves with different time steps and stabilization constants for the PFC model

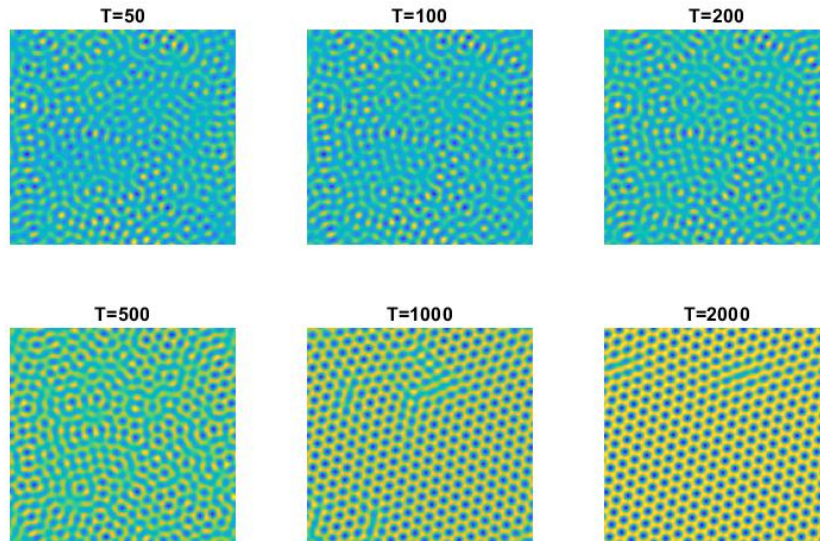


Figure 8: ETDRK3 solutions for the PFC model with $\beta = 3, \tau = 0.1$ at $T=50, 100, 200, 500, 1000, 2000$

The energy curves with different time steps and stabilization constants are shown in Fig. 9. There are 5 curves in total and 4 of them overlap. With $\beta = 3$, the solution is good when $\tau = 0.1$, but when $\tau = 1$, the time delay caused by the stabilization is much more severe, which indicate that we should not use any stabilization when computing with large time steps. However, it is remarkable that ETDRK3 without stabilization performs very well even with the time step as

large as $\tau = 10$.

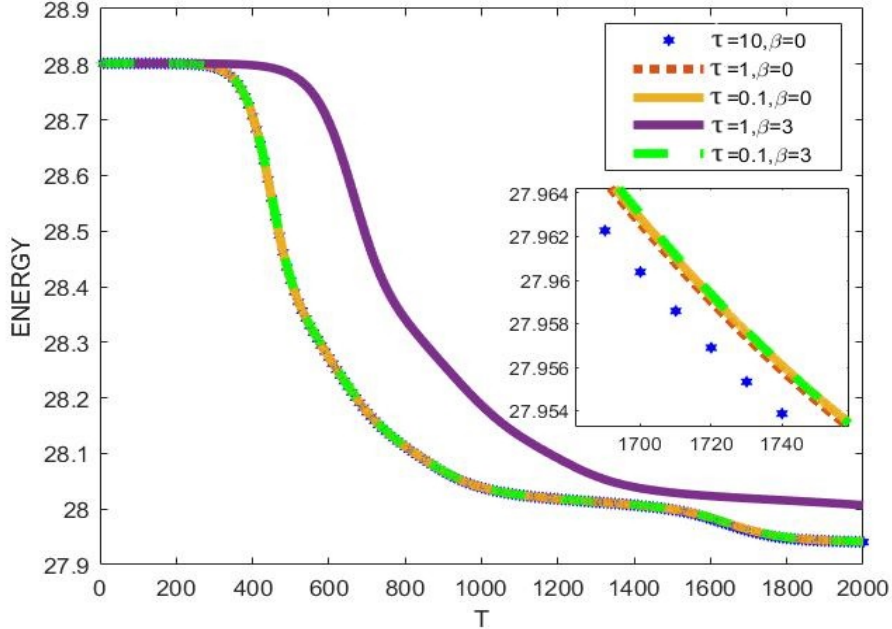


Figure 9: Energy curves with different time steps and stabilizers

4.5 Adaptive time stepping

Solutions of gradient flows may vary drastically during some short time intervals, but only slightly at other times. A main advantage of unconditional energy stable schemes is that they can be easily used to construct an adaptive time stepping algorithm, in which the time step is only dictated by accuracy rather than by stability. There are often essential difficulties in applying adaptive time-stepping strategies to other schemes, since most of them do not have robust unconditionally stability with variable step sizes. This is also where the significance of the high-order unconditionally energy stable schemes lies.

For gradient flows, there are several adaptive time stepping strategies, see [2, 13, 23, 36]. Here we make use of the strategy in [24] summarized in the following Algorithm 1. In Step 4 and 6, the time step size which needs to update is given by the formula

$$A_{dp}(e, \tau) = \rho \left(\frac{tol}{e} \right)^r \tau, \quad (4.2)$$

along with the restriction of the minimum and maximum time steps. In the above formula, ρ is a default safety coefficient, tol is a reference tolerance to be set, e is the relative error computed at each time level in Step 3 and r is the adaptive rate to be set. In our numerical example, we set $\rho = 0.9$ and $tol = 5 * 10^{-3}$, the minimum time step to be 10^{-4} and the maximum time step to be $\tau = 10^{-2}$ for Fig. 6 and Fig. 7 and $\tau = 10^{-1}$ for Fig. 8 and 9. The initial time step is taken as the minimum time step.

Algorithm 1 Adaptive time stepping procedure

Given: U^n, τ_n

Step 1. Compute U_1^{n+1} by the first-order ETD scheme with τ_n .

Step 2. Compute U_2^{n+1} by the third-order ETDRK scheme with τ_n .

Step 3. Calculate $e_{n+1} = \frac{\|U_1^{n+1} - U_2^{n+1}\|}{\|U_2^{n+1}\|}$.

Step 4. If $e_{n+1} > tol$, recalculate the time step $\tau_n \leftarrow \max\{\tau_{min}, \min\{A_{dp}(e_{n+1}, \tau_n), \tau_{max}\}\}$,

Step 5. goto Step 1.

Step 6. else, update the time step $\tau_{n+1} \leftarrow \max\{\tau_{min}, \min\{A_{dp}(e_{n+1}, \tau_n), \tau_{max}\}\}$.

Step 7. endif

We take the two-dimensional Cahn–Hilliard equation as an example to examine the performance of the adaptive time stepping algorithm. We take $\epsilon = 0.1$, $N = 512$, $\beta = 2$ and $r = 1/3$. As comparison, we compute two ETDRK3 solutions with a small uniform time step $\tau = 10^{-4}$ and large uniform time step $\tau = 10^{-2}$ as references.

We plot in Fig. 10 the energy curves (left) and the size of adaptive time steps (right). We observe that solution obtained with $\tau = 10^{-2}$ is not accurate, while the adaptive time stepping solutions are in excellent agreement with the small time step solution with $\tau = 10^{-4}$. In addition, except at the initial time period and two other small time intervals where the energy varies drastically, the adaptive time steps basically stay around $\tau = 10^{-2}$. Finally, we plot in Fig. 11 snapshots of the phase evolution at different times.

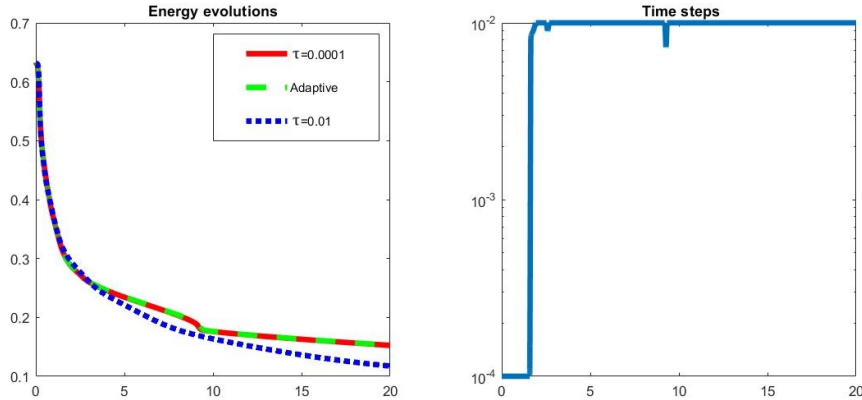


Figure 10: Energy curves among small time steps $\tau = 0.0001$, adaptive time steps and large time steps $\tau = 0.01$ and the size of time steps in the adaptive procedure

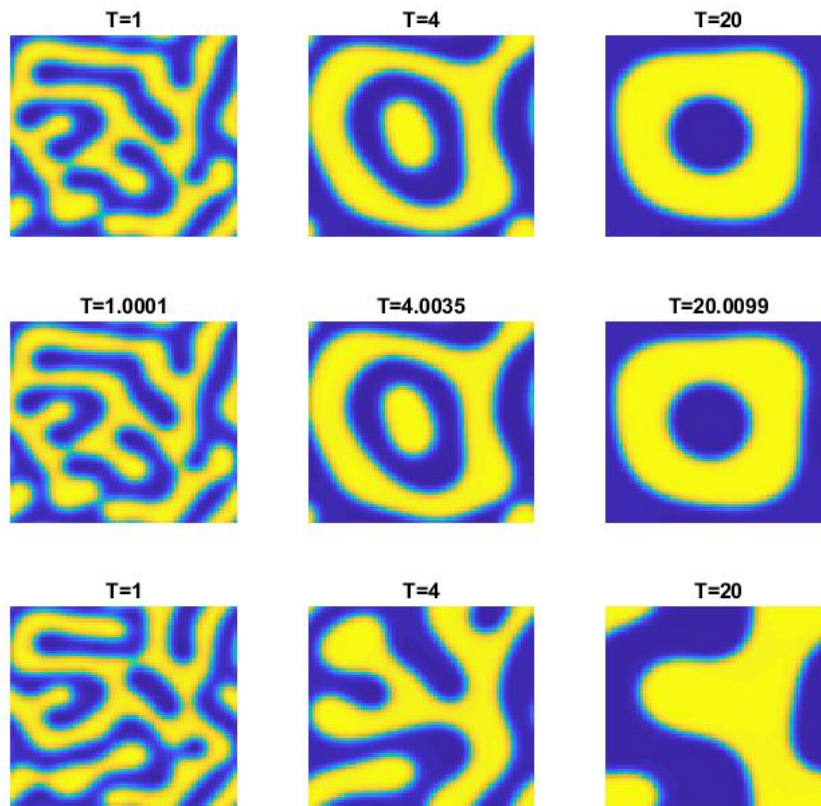


Figure 11: Solutions for the Cahn–Hilliard equation using small time steps $\tau = 0.0001$ (first line), adaptive time steps (second line) and large time steps $\tau = 0.01$ (third line)

5 Concluding Remarks

We derived in this paper an general framework to construct arbitrary high order and unconditional energy stable ETDRK schemes for a class of gradient flows, and identified a set of conditions that need to be satisfied for a ETDRK scheme to be unconditional energy stable. In particular, we showed that commonly used third-order and fourth-order ETDRK schemes are not unconditional energy stable, and constructed new third-order ETDRK schemes which are unconditional energy stable.

To the best of our knowledge, this is the first result on higher than second-order unconditional energy stable ETDRK schemes. Here are some extensions and future work to consider:

- Higher-order: While we provided a set of conditions that ETDRK schemes need to satisfy in order to be unconditional energy stable. But due to the complexity of these conditions, the existence of higher than third-order ETDRK unconditionally energy stable schemes is still an open question. One possibility is to add one more stage which will lead to more free parameters to choose from.

- Other models: We restricted ourselves to a class of gradient flows with Lipschitz nonlinearities. Since the ETDRK schemes are based on the Duhamel’s Principle so the only error comes from the numerical integration, we expect that the new ETDRK schemes behave well for many other models with even more complicated physical structures, although proving rigorously unconditional energy stability for more complicated models would be a challenge.

We are hopeful that our results in this paper can be extended to more general systems and to higher than third-order ETDRK schemes.

Acknowledgements

J. Shen and Z. Fu are partially supported by NSFC 12371409. J. Yang is supported by the National Natural Science Foundation of China (NSFC) Grant No. 12271240, the NSFC/Hong Kong RGC Joint Research Scheme (NSFC/RGC 11961160718), and the Shenzhen Natural Science Fund (No. RCJC20210609103819018).

References

- [1] G. AKRIVIS, B. LI, AND D. LI, *Energy-decaying extrapolated RK-SAV methods for the Allen–Cahn and Cahn–Hilliard equations*, SIAM J. Sci. Comput., 41 (2019), pp. A3703–A3727.
- [2] W. CHEN, Y. Y. X. WANG, AND Z. ZHANG, *A second order BDF numerical scheme with variable steps for the Cahn–Hilliard equation*, SIAM J. Numer. Anal., 57 (2019), pp. 495–525.
- [3] Q. CHENG, C. LIU, AND J. SHEN, *A new Lagrange multiplier approach for gradient flows*, Comput. Method Appl. M., 367 (2020), p. 113070.
- [4] Q. CHENG AND J. SHEN, *Multiple scalar auxiliary variable (MSAV) approach and its application to the phase-field vesicle membrane model*, SIAM J. Sci. Comput., 40 (2018), pp. A3982–A4006.
- [5] S. M. COX AND P. C. MATTHEWS, *Exponential time differencing for stiff systems*, J. Comput. Phys., 176 (2002), pp. 430–455.
- [6] Q. DU, L. JU, X. LI, AND Z. QIAO, *Maximum principle preserving exponential time differencing schemes for the nonlocal Allen–Cahn equations*, SIAM J. Numer. Anal., 57 (2019), pp. 875–898.
- [7] Q. DU, L. JU, X. LI, AND Z. QIAO, *Maximum bound principles for a class of semilinear parabolic equations and exponential time differencing schemes*, SIAM Rev., 63 (2021).
- [8] Q. DU AND W. ZHU, *Stability analysis and application of the exponential time differencing schemes*, J. Comput. Math., 22 (2004), pp. 200–209.
- [9] D. J. EYRE, *An unconditionally stable one-step scheme for gradient systems*, unpublished, <http://www.math.utah.edu/eyre/research/methods/stable.ps>, (1997).

- [10] X. FENG, T. TANG, AND J. YANG, *Long time numerical simulations for phase-field problems using p -adaptive spectral deferred correction methods*, SIAM J. Sci. Comput., 37 (2015), pp. A271–A294.
- [11] Z. FU AND J. YANG, *Energy-decreasing exponential time differencing Runge–Kutta methods for phase-field models*, J. Comput. Phys., 454 (2022).
- [12] H. GOMEZ AND T. HUGHES, *Provably unconditionally stable, second-order time-accurate, mixed variational methods for phase-field models*, J. Comput. Phys., 230 (2011), pp. 5310–5327.
- [13] Y. HE, Y. LIU, AND T. TANG, *On large time-stepping methods for the Cahn–Hilliard equation*, Appl. Numer. Math., 57 (2006), pp. 616–628.
- [14] M. HOCHBRUCK AND A. OSTERMANN, *Explicit exponential Runge-Kutta methods for semi-linear parabolic problems*, SIAM J. Numer. Anal., 43 (2006), pp. 1069–1090.
- [15] M. HOCHBRUCK AND A. OSTERMANN, *Exponential integrators*, Acta Numerica, 19 (2010), pp. 209–286.
- [16] D. HOU AND Z. QIAO, *An implicit–explicit second-order bdf numerical scheme with variable steps for gradient flows*, J. Sci. Comput., 94(2) (2023), p. 39.
- [17] F. HUANG AND J. SHEN, *A new class of implicit–explicit BDFk SAV schemes for general dissipative systems and their error analysis*, Comput. Method Appl. M., 392 (2022), p. 114718.
- [18] L. JU, X. LI, AND Z. QIAO, *Generalized sav-exponential integrator schemes for allen–cahn type gradient flows*, SIAM J. Numer. Anal., 60(4) (2022), p. 1905–1931.
- [19] S. KROGSTAD, *Generalized integrating factor methods for stiff PDEs*, J. Comput. Phys., 203 (2005), pp. 72–88.
- [20] B. LI AND J. LIU, *Thin film epitaxy with or without slope selection*, European J. Appl. Math., 14 (2003), pp. 713–743.
- [21] D. LI, Z. QIAO, AND T. TANG, *Characterizing the stabilization size for semi-implicit Fourier-spectral method to phase field equations*, SIAM J. Numer. Anal., 54 (2016), pp. 1653–1681.
- [22] X. LI, Z. QIAO, AND C. WANG, *Convergence analysis for a stabilized linear semi-implicit numerical scheme for the nonlocal Cahn–Hilliard equation*, Math. Comp., 90 (2021), pp. 171–188.
- [23] F. LUO, T. TANG, AND H. XIE, *Parameter-free time adaptivity based on energy evolution for the Cahn–Hilliard equation*, Commun. Comput. Phys., 19 (2016), pp. 1542–1563.
- [24] J. SHEN, T. TANG, AND J. YANG, *On the maximum principle preserving schemes for the generalized Allen–Cahn equation*, Comm. Math. Sci., 14 (2016), pp. 1517–1534.

- [25] J. SHEN, C. WANG, X. WANG, AND S. WISE, *Second-order convex splitting schemes for gradient flows with Ehrlich-Schwoebel type energy: Application to thin film epitaxy*, SIAM J. Numer. Anal., 50 (2012), pp. 105–205.
- [26] J. SHEN, J. XU, AND J. YANG, *The scalar auxiliary variable (SAV) approach for gradient flows*, J. Comput. Phys., 353 (2018), pp. 407–416.
- [27] J. SHEN, J. XU, AND J. YANG, *A new class of efficient and robust energy stable schemes for gradient flows*, SIAM Rev., 61 (2019), pp. 474–506.
- [28] J. SHEN AND X. YANG, *Numerical approximations of Allen–Cahn and Cahn–Hilliard equations*, Discret. Contin. Dyn. Syst., 28 (2010), pp. 1669–1691.
- [29] J. SHIN, H. G. LEE, AND J. Y. LEE, *Convex splitting Runge-Kutta methods for phase-field models*, Comput. Math. with Appl., 73 (2017), pp. 2388–2403.
- [30] T. TANG, *Revisit of semi-implicit schemes for phase-field equations*, Anal. Theory Appl., 36(3) (2020), pp. 235–242.
- [31] T. TANG, X. WU, AND J. YANG, *Arbitrarily high order and fully discrete extrapolated RK-SAV/DG schemes for phase-field gradient flows*, J. Sci. Comput., 93 (2022).
- [32] T. TANG AND J. YANG, *Implicit-explicit scheme for the Allen–Cahn equation preserves the maximum principle*, J. Comput. Math., 34 (2016), pp. 451–461.
- [33] C. XU AND T. TANG, *Stability analysis of large time-stepping methods for epitaxial growth models*, SIAM J. Numer. Anal., 44 (2006), pp. 1759–1779.
- [34] X. YANG, *Linear, first and second-order, unconditionally energy stable numerical schemes for the phase field model of homopolymer blends*, J. Comput. Phys., 327 (2016), pp. 294–316.
- [35] X. YANG, J. ZHAO, Q. WANG, AND J. SHEN, *Numerical approximations for a three-component Cahn–Hilliard phase-field model based on the invariant energy quadratization method*, Math. Models Methods Appl. Sci., 27 (2017), pp. 1993–2030.
- [36] Z. ZHANG AND Z. QIAO, *An adaptive time-stepping strategy for the Cahn–Hilliard equation*, Commun. Comput. Phys., 11 (2012), pp. 1261–1278.